N 72-25543

NASA TECHNICAL MEMORANDUM

NASA TM X-68052

NASA TM X-68052

EXPLORATION OF ALLOY SURFACE AND SLURRY MODIFICATION TO IMPROVE OXIDATION LIFE OF FUSED SILICIDE COATED NIOBIUM ALLOYS

by S. R. Levine
U.S. Army Air Mobility Research and Development Laboratory
NASA - Lewis Research Center
Cleveland, Ohio

and

S. J. Grisaffe
Lewis Research Center
Cleveland, Ohio

TECHNICAL PAPFR proposed for presentation at the
Refractory Metal Coatings Session of the Metallurgical Society -
American Institute of Mining, Metallurgical, and Petroleum Engineers Meeting
Boston, Massachusetts, May 8-11, 1972

EXPLORATION OF ALLOY SURFACE AND SLURRY MODIFICATION TO IMPROVE OXIDATION LIFE OF FUSED SILICIDE COATED NIOBIUM ALLOYS

by S. R. Levine and S. J. Grisaffe

E-6751

ABSTRACT

Edge and surface modification of niobium alloys prior to coating with Si-20Cr-20Fe and slurry composition modification were investigated to improve performance in a 1370°C ambient pressure slow-cycle test. The best coating obtained was Si-20Cr-20Mn with an average life of 63 cycles compared to 40 for Si-20Cr-20Fe on FS-85 (100 percent improvement in weight parity life). Edge beading extended the lives of Si-20Cr-20Fe coated Cb-752 and FS-85 to 57 and 41 cycles respectively (50 and 20 percent improvements in weight parity life respectively). W, Al_2O_3 and $ZrO_2 \cdot CaO$ surface modifications altered coating crack frequency and microstructure and increased life somewhat.

EXPLORATION OF ALLOY SURFACE AND SLURRY MODIFICATIONS TO IMPROVE OXIDATION LIFE OF FUSED SILICIDE COATED NIOBIUM ALLOYS

by S. R. Levine and S. J. Grisaffe
National Aeronautics and Space Administration
Lewis Research Center
Cleveland, Ohio

SUMMARY

Surface modification of two niobium alloys prior to coating with Si-20Cr-20Fe was investigated as a technique for altering the coating microstructure and crack frequency so as to improve the performance of the coated systems. The feasibility of reducing susceptibility to edge failure by electron-beam melting an edge bead on thin sheet specimens prior to application of the fused slurry silicide coating was investigated. Also, W. Al_2O_3 or $ZrO_2 \cdot CaO$ alloy surface modifiers were applied by several methods prior to silicide coating. In addition, a number of slurry composition modifications were investigated. These were intended to alter coating structure, oxidation behavior, and glass forming ability.

The applied coatings were screened by a 1370°C, one-hour slow-cycle test at ambient pressure. To be conservative, appearance of the first Nb_2O_5 pimple was used as the coating failure

criterion. Vendor and in-house Si-20Cr-20Fe coatings were used as a baseline for comparison. Coatings were compared on an absolute and on a weight parity basis (coating life in cycles divided by the coating weight in mg/cm^2). The baseline R512E coating had an average life of 40 cycles on FS-85 (weight parity life of 1.6) and 48 cycles on Cb-752 (weight parity life of 2.0).

Edge beading reduced susceptibility to edge failure of coated Cb-752 and FS-85. On a weight parity basis, 50 and 20 percent improvements in life were realized over R512E on unmodified Cb-752 and FS-85 respectively.

W, Al_2O_3, and $ZrO_2 \cdot CaO$ alloy surface modifiers successfully altered the crack frequency and microstructure of Si-20Cr-20Fe but improved life by no more than 25 percent on a weight parity basis.

The best slurry chemistry modification coating on FS-85 was Si-20Cr-20Mn which formed a glassy surface oxide. This coating gave an average life of 63 cycles (a weight parity life of 3.2 which is a 100 percent improvement over R512E).

INTRODUCTION

Fused slurry silicide coatings have the potential for providing reliable oxidation protection for niobium alloy re-entry heat shields and aircraft gas turbine combustors and vanes (1-5). Because the relatively brittle silicide coatings have a higher thermal expansion coefficient than the niobium alloy substrates,

a natural crack pattern develops in these coatings upon cooling from the coating firing temperature (6). The cracks are generally oriented perpendicular to the substrate with a spacing comparable to the coating thickness. Thus, the crack network which develops in the coatings is quite extensive. Even though these cracks may partially close on heating, they offer paths for atmospheric oxygen to penetrate deep into the coating. Oxide formation in these cracks eventually leads to localized coating breakdown and substrate oxidation. This can be detected visually by the growth of niobium oxide pimples. The appearance of the first oxide pimple provides a conservative determination of coating life since structural failures due to oxidation/oxygen embrittlement usually occur after considerably longer times. The edges of thin sheet components, such as heat shield panels, are particularly prone to such localized coating breakdowns (7).

The first major purpose of this study was to explore several methods for modifying the surface of niobium alloys to produce coatings with longer lives as a result of altered natural crack frequency and microstructure. Two approaches were taken. First, the edge geometry of thin sheet specimens was modified so as to increase the edge radius therby reducing the alteration in coating structure and the high tensile stresses caused by corners. This was accomplished by electron beam melting the edges of Cb-752 and FS-85 specimens. Second, attempts were made to alter the

microstructure and reduce the thermal expansion coefficient of the silicide coatings so as to minimize the number of tensile cracks. The approach for accomplishing this was to provide dispersed nucleation sites at the substrate surface or in the coating by introducing an additional phase, preferably with a lower thermal expansion coefficient than that of the coating. Dispersed nucleation sites would tend to randomize the columnar structure of the coating therby reducing the number of short length grain boundaries offering potentially harmful crack paths to the substrate. Second phases with lower thermal expansion coefficients than the coating would tend to reduce the net thermal expansion coefficient of the coatings by a rule of mixtures effect. These studies were conducted on alloy FS-85.

The second major purpose of this study was to investigate slurry modifications. These were directed toward physical changes in the coatings as discussed previously as well as toward modifying the oxidation kinetics of the coating and its ability to form a glassy oxide.

The coatings were tested by slow-cycle ambient pressure oxidation to 1370°C to evaluate the effect of beading the edges of Cb-752 and FS-85 specimens, modification of the alloy surface of FS-85 specimens with tungsten (W), alpha alumina (Al_2O_3), or partially stabilized zirconia (ZrO_2-5W/oCaO), and slurry modification. The slow-cycle test to 1370°C in ambient pressure air is a

severe one for this system since the normal maximum use temperature is about 1320°C in reduced pressure environments and about 1250°C in ambient pressure air. Commercial and unmodified Si-20Cr-20Fe fused slurry silicide coatings were used as a baseline for comparison. Coatings were compared on a weight parity basis, that is, the coating life in cycles divided by the coating weight in milligrams per square centimeter. The basis for such a comparison is well established since, for a given silicide coating, life is proportional to coating weight (1).

In addition to comparing the time to first visible local coating breakdown, supporting metallographic and bend tests were used to evaluate some of the coatings. Some supplemental electron microprobe (EMP) coating characterization was also conducted.

Materials Selection

Niobium alloys Cb-752 (Nb-9W-2.7Zr with 120 ppm O_2) and FS-85 (Nb-28Ta-11W-1Zr with 240 ppm O_2) were used as substrates in this study. Both alloys were in the form of thin gage sheet (approximately 0.030 cm or 12 mils) in the 100 percent recrystallized condition. These alloys and this thickness range are of interest for re-entry vehicle heat shield applications.

Silicon (-325 mesh), chromium (-325 mesh), and iron (-0.5 micron) powders of greater than 99 percent purity were used to form the basic fused slurry silicide coating, Si-20Cr-20Fe. This coating was selected because its commercial counterpart (Sylvania

R512E) is a primary candidate for protection of niobium alloy heat shields. Sylvania R512E coated specimens were used as a baseline for this study. Figure 1 shows the cross sectional microstructures of R512E coated Cb-752 and FS-85 and gives an indication of the frequency and depth of cracks to be found in these coatings in the as-coated conditions. Also, the thinning of the outer protective layers at the edges in the 100X micrographs should be noted.

The alloy surface modifiers examined were W (-4.5 micron powder), Al_2O_3 (-325 mesh), and ZrO_2-5 wt% CaO (-325 mesh). The W was greater than 99.5 percent pure and the oxide powders were greater than 98 percent pure. The modifiers were applied by four methods: roll bonding, flame spraying, isostatic pressing, and slurry spraying. The four techniques offered varying degrees of bonding between the modifier and the substrate and were expected to produce different modifier distributions when reacted with Si-20Cr-20Fe. The reasons for selecting these modifiers are presented schematically in figure 2.

Silicides generally have larger thermal expansion coefficients than their parent metals. Niobium alloys have thermal expansion coefficients in the range 7 to 8 x 10^{-6} cm/cm-^{o}C whereas the thermal expansion coefficient for $NbSi_2$ is reported to be from 7.3 to 11.7 x 10^{-6} cm/cm-^{o}C (7-9). This difference in thermal expansion coefficients is believed to be the source of tensile

coating cracks as shown schematically in figure 2(a). Tungsten was selected as a modifier because, in addition to providing dispersed mucleation sites for disruption of the columnar structure (fig. 2(b)), the disilicide of tungsten with a thermal expansion coefficient of about 7.9×10^{-6} cm/cm-^{o}C (10) may be an effective additive for reducing the thermal expansion coefficient of the coating (fig. 2(c)). Also, solid solutions of WSi_2 and $NbSi_2$ have smaller molar volumes than $NbSi_2$(11).

Al_2O_3 and $ZrO_2 \cdot CaO$ were selected for their high thermodynamic stability, dispersed nucleation site capabilities, and possibly favorable thermal expansion effects. α-Al_2O_3 has a linear thermal expansion coefficient of about 8×10^{-6} cm/cm-^{o}C (12). Addition of 25 percent Al_2O_3 to $MoSi_2$ reportedly gave a composite with a thermal expansion coefficient of 7.3×10^{-6} compared with 8.7×10^{-6} for $MoSi_2$ (12). The same effect may be operative with Al_2O_3 and $NbSi_2$. Partially stabilized zirconia transforms from a mixture of cubic and monoclinic phases to a single tetragonal phase at about 1000^{o}C (13). On heating (fig. 2(d)), the coefficient of thermal expansion is about 7×10^{-6} cm/cm-^{o}C until the transformation temperature. At this point the coefficient becomes negative until the transformation is completed. Then, approximately the same rate of expansion is resumed. On cooling the process is reversed forming a hysteresis loop (12). Based on the rule of mixtures, this behavior should lower the net

thermal expansion coefficient of the composite coating, especially in the intermediate temperature range, thereby reducing the number of tensile cracks and thus potential oxidation paths.

Slurry modifiers were selected for a wide variety of reasons including those already discussed. The oxide modifiers ZrO_2-5 wt% CaO, HfO_2, and Al_2O_3 (all -325 mesh, > 98 percent purity) were selected for their thermal expansion properties and dispersed nucleation site capabilities. The B_4Si (-200 mesh, > 98 percent purity) and Mn (-325 mesh, > 99 percent purity) (18) modifiers were selected for their glass forming capabilities. Depending on oxygen partial pressure, a liquid is present in the Mn-Si-O system at temperatures as low as 1210°C as a eutectic formed between $MnSiO_3$ and Mn_2SiO_4. Although FeO-SiO_2 forms a slightly lower melting oxide (Fe_2SiO_4 at 1200°C), the appearance of this phase is limited due to the relative instability of FeO (13, 16). Additions of W (-4.5 u, > 99.5 percent purity), Mo (-325 mesh, > 99 percent purity), and VSi_2 (-325 mesh, > 98 percent purity) were aimed at approaching the Si/50W-20Mo-15Ti-15V coating developed at Solar under NASA contract (17) by a fused slurry approach. Nb (-325 mesh, > 99 percent purity) was used as an additive to suppress the substrate-slurry reaction so as to minimize loss of sheet thickness and to provide dispersed nucleation sites. Co (-2.3 u, > 99 percent purity), Zr (-200 mesh, > 99 percent purity), Hf (-325 mesh, > 99 percent purity), and aluminide modifiers

(NiAl:-60 mesh, > 98 percent purity; CoAl:-100 mesh, > 98 percent purity) were added to give a coating with a more even oxidation rate as a function of temperature and/or to take advantage of the favorable thermal expansion properties of HfO_2, ZrO_2, or Al_2O_3.

EXPERIMENTAL PROCEDURE

Specimen Preparation and Oxidation

Cb-752 and FS-85 coupons (3.8 x 1.9 cm x approximately 0.030 cm thick) were sheared with the long dimension parallel to the sheet rolling direction. A hole (0.48 cm diameter) was drilled near one end and the coupons were jar milled in an alumina slurry to round off edges and corners. The Cb-752 and some FS-85 specimens were further prepared by electron beam melting a bead along the external edges as shown for Cb-752 in the cross-section photomicrograph in figure 3 (100X). The bead diameters were approximately 1.6 and 2.3 times the sheet thickness for Cb-752 and FS-85 respectively. All coupons were grit blasted with Al_2O_3, rinsed in water, measured, degreased, rinsed in distilled water and weighed to the nearest 0.1 mg.

Surface modification was performed in four different ways: (1) slurry sprayed modifier application using a nitrocellulose lacquer binder, (2) roll bonding following slurry spray application, (3) isostatic pressing at 275 MN/m^2 (20 ksi) after slurry spraying and wrapping in mylar (14), and (4) flame spraying with an oxyacetylene torch.

After surface modification, the specimens were re-weighed and measured. The data are reported in Table I. The specimens were then oversprayed with the Si-20Cr-20Fe slurry, re-weighed, and measured as shown in Table I. The green coatings were fused and annealed at 1420°C for one hour at a pressure below 2×10^{-4} torr once initial outgassing of the binder subsided. The specimens were weighed and measured after the firing cycle as shown in Table I.

Coating chemistry modifications were applied on FS-85 in a single step per side by spraying with the nitrocellulose lacquer vehicle. Edge and substrate preparation were the same as discussed previously. The specimens were air dried and weighed before and after firing. Firing was conducted either in vacuum or dry argon as indicated in Table II. The time at peak temperature was one hour.

Slow-cycle ambient pressure oxidation tests were conducted in a vertical mullite tube furnace controlled to $\pm$ 10°C. The specimens were exposed to temperatures above 1320°C for about 28 minutes of each one hour cycle and to a maximum temperature of 1370°C for about ten minutes. The minimum temperature in each cycle was about 100°C. The specimens were visually examined every few cycles and weighed once per day. The appearance of the first Nb_2O_5 pimple was considered the time to local coating breakdown and the specimen was removed from test. This is a very conserva-

tive estimate of useful life since specimens and parts with intentionally defected coatings have not shown rapid failures after several cycles of simulated re-entry exposure (ref. 4).

Additional Evaluations

Representative samples of each coating were examined by metallography in the as-coated condition. Electron microprobe (EMP) raster photomicrography was used to determine surface modifier distributions in the as-fused coatings. Coating cracks were counted on 100X cross sectional micrographs in the as-coated condition. A crack was defined as a fissure extending from the diffusion zone to the coating surface for counting purposes. Also, some samples were examined by metallography after test. Oxides were analyzed by X-ray diffraction (XRD) techniques either in situ or on scrapings.

Selected samples were bend tested in the as-coated condition and after exposure. Bend specimens cut from the coupon specimens were half the coupon width by the full length (0.9 cm x 3.8 cm). The specimens were bent over a 0.20 cm radius roller (approximately four times the coated thickness of the specimens) at a crosshead speed of 2.5 cm/min. In most cases an approximate ductile-brittle transition temperature was assigned by inspection of the bend angle at fracture and interpolation because the number of specimens tested was not sufficient to accurately determine the DBTT.

RESULTS AND DISCUSSION

Data for the evaluation and testing of the vendor and in-house coatings are summarized in the right-hand columns of Tables I, II, and III. The data listed generally include coating weight, coating thickness, coating crack frequency, lives observed in the 1370°C ambient pressure slow-cycle test, life on a weight parity basis, and estimated ductile-brittle transition temperatures. The weight parity life, defined as coating life in cycles divided by coating weight in mg/cm^2, was included to permit comparison of systems with different coating weights. Based on earlier results, coating life is, to a good approximation, proportional to coating weight for a given coating composition (1). Therefore, comparisons of different coatings on a weight parity basis are valid.

Edge Beading

The baseline systems for this study were R512E on Cb-752 and FS-85 as shown in figure 1.

The unmodified in-house Si-20Cr-20Fe coating on edge-beaded Cb-752 (fig. 4(a), 4(b)) is very similar in microstructure to R512E on Cb-752. The in-house coating is considerably thinner (0.06 mm vs 0.09 mm based on metallographically determined coating thicknesses). The in-house Si-20Cr-20Fe coating on FS-85 (fig. 4(c), (d)) appears to be slightly denser than R512E on FS-85 (fig. 1(c), (d)). Also, the outer two-phase region consists of coarser, more equiaxed grains than are found in R512E. The in-house coating is thinner (0.075 mm vs 0.09 mm based on metallo-

graphically determined coating thicknesses) and has a slightly higher natural crack frequency than the R512E coating.

As can be seen from Table I, edge beading of Cb-752 gave about 20 percent longer life than the average for R512E on Cb-752. This was accomplished with a 20 percent lighter coating. On a weight parity basis, the improvement resulting from edge beading is about 50 percent. Edge beading of FS-85 gave no improvement of life on an absolute basis. This may be due to the fact that the edge beads on FS-85 were less uniform and exhibited local interruptions. However, since the coating weight was about 20 percent lighter, the improvement on a weight parity basis is about 20 percent. The statistical baseline coating performance and the magnitude of the improvements due to edge beading are illustrated in figure 5. The statistical distribution of lives for the baseline coatings are illustrated by the Weibull plots (15) of percent cumulative failures versus weight parity life in figure 5(a), (b). For the 95 percent, 50 percent, and 5 percent confidence lines, the true coating life has 95 percent, 50 percent, or 5 percent probability of being higher than the lives shown respectively. The knee on figure 5(b) reflects early random failures. The observed lives for edge beaded Cb-752 and FS-85 lie at or above the 5 percent line. Absolute and weight parity lives are compared in the top four bars of figure 5(c). The distribution of observed weight parity lives are also shown here to

permit a more detailed comparison. Longer lives generally were obtained because of the reduced susceptibility to edge failure which results from the larger edge radius produced by edge beading. The change in substrate microstructure produced by beading appeared to have no deleterious effect on coating performance. Both R512E and Si-20Cr-20Fe maintained Cb-752 substrate ductility as revealed by bend tests. Such tests were not conducted on FS-85.

Surface Modifiers

The baseline systems for this part of the work were R512E on FS-85 and its unmodified Si-20Cr-20Fe in-house counterpart. Coating lives observed in the 1370°C slow-cycle test (table I) were slightly greater for R512E than for in-house Si-20Cr-20Fe on an absolute basis. However, on a weight parity basis the cycles to first local coating breakdown obtained with the two coatings were about the same. Note that R512E on FS-85 gave weight parity lives about 20 percent lower than R512E on Cb-752. Both coatings maintained substrate ductility as revealed by bend tests.

Photomicrographs of Si-20Cr-20Fe on alloy surface modified FS-85 in the as-coated condition are presented in figure 6, 7, and 8. Coating evaluation data are summarized in Table I.

The Al_2O_3 surface modifications (fig. 6) had the greatest effect on coating crack frequency. In all cases, the crack fre-

quency was increased and the microstructure of the outer strata of the coatings was refined. The flame spray modification which had the greatest amount of Al_2O_3 had the highest crack frequency: 28 cracks/mm compared to 16 cracks/mm for unmodified Si-20Cr-20Fe. In all cases Al_2O_3 was distributed uniformly in the lower strata of the coatings but was most concentrated in the outer strata as revealed by polarized light metallography.

The flame sprayed Al_2O_3 modification gave the best lives for this series of coatings (42 and 46 cycles). On a weight parity basis, this represents a 25 percent improvement over the performance of unmodified Si-20Cr-20Fe. Substrate ductility was maintained as revealed by bend test results. Several of the other application techniques gave long but nonrepeatable lives. This behavior may be associated with variability in the modifier application step.

The $ZrO_2 \cdot CaO$ modifications (fig. 7) had a relatively small effect on coating crack frequency with the exception of the flame spray modification. For this modification, the $ZrO_2 \cdot CaO$ content was highest and the crack frequency was reduced from 16 cracks per mm to about 9 cracks per mm. $ZrO_2 \cdot CaO$ additions tended to increase the extent of the columnar region of the coating adjacent to the substrate and to increase the grain size in the outer strata of the coating. EMP raster micrographs revealed that $ZrO_2 \cdot CaO$ was concentrated in the columnar region and near the outer surface

in all cases but the slurry spray application where the concentration was uniform.

The flame spray application gave the best lives for the $ZrO_2 \cdot CaO$ modifications (47 and 49 cycles). On a weight parity basis and on an absolute basis a 20 percent improvement over unmodified Si-20Cr-20Fe was achieved. Excellent substrate ductility was maintained as revealed by bend test results. Other $ZrO_2 \cdot CaO$ applications gave long but nonrepeatable lives. Again, this is probably associated with variability in the modifier application technique.

The magnitude of the improvements can be established in figure 5. The observed lives for the flame-sprayed Al_2O_3 and $ZrO_2 \cdot CaO$ modifications would lie beyond the 5 percent line for unmodified Si-20Cr-20Fe (fig. 5(b)). The magnitude of the improvements on an absolute and weight parity basis are compared in figure 5(c).

The W surface modifications (fig. 8) had a relatively small effect on coating crack frequency with the exception of the roll bonded modification where the crack frequency was increased to 20 per mm. This group of coatings had a more distinctly stratified structure and coarser grains than unmodified Si-20Cr-20Fe. Based on EMP raster photomicrographs, W was concentrated primarily in the outer light etching layer of the coating. However, the W concentration throughout these coatings was higher than in unmodified coatings where W is picked up only by reaction with the substrate.

The isostatically pressed W modification gave the best average life of all alloy surface modified coatings (51 cycles). However, on a weight parity basis, life was only comparable to unmodified Si-20Cr-20Fe on FS-85. Substrate ductility was maintained as revealed by bend test results. Flame spraying and roll bonding produced uneven coatings. However, one roll bonded specimen performed well. Slurry spraying gave even coatings but these performed poorly.

Modifier contents expressed in terms of volume percent of the as-fused coatings are listed in Table I. Some trends between modifier content and crack frequency were noted as shown in figure 9(a) for the W and $ZrO_2 \cdot CaO$ modifications. In both cases, as modifier content was increased crack frequency generally decreased. Extrapolation to a crack-free coating shows modifier contents of 20 and 12 volume percent are required for W and $ZrO_2 \cdot CaO$ respectively. For Al_2O_3 additions the relationship between crack frequency and additive content was not clear. A strong trend between crack frequency (or modifier content) and coating life was not evident for the Al_2O_3 and W modifications. This is probably due to variations in modifier distributions or to poor repeatability resulting from the four modifier application techniques used. For the $ZrO_2 \cdot CaO$ modification, there may be an increase in life with decreasing crack frequency as shown by the least mean squares line drawn through the observed lives in figure 9(b).

Photomicrographs of R512E on FS-85 and the three best coatings for each surface modifier after exposure to the 1370°C slow-cycle test are presented in figure 10. In all cases oxide has grown in the natural coating cracks and the cracks have widened. The amount of growth was least for W modified Si-20Cr-20Fe. This reduced the amount of coating crack formation in the diffusion zone (the dark etching layer adjacent to the substrate). Diffusion zone cracks running parallel to the substrate can be particularly damaging to the integrity of the coating. The diffusion zone grew in all cases from about 4 microns as-coated to about 12 microns after test. The net coating thickness was reduced by about 16 microns for R512E and the Al_2O_3 and $ZrO_2 \cdot CaO$ modifications and about 24 microns for the W modification.

The oxides formed on the modified coatings appear to be more voluminous than on R512E and appear to contain more of the lighter oxide phase. This phase was blue under a sensitive tint filter and black under polarized light. The major oxide phase was rust colored under polarized light. Based on the results of XRD analysis of scrapings from the four specimens the latter phase was identified as an (Fe, Cr) NbO_4 and the former phase was α-cristobalite. Additional minor phases detected by XRD were Cr_2O_3 in the $ZrO_2 \cdot CaO$ modification and Nb_2O_5 in the W modification. However, the green Cr_2O_3 phase was observed under polarized light in the oxides on all four coatings. It was located in some of the

cracks and adjacent to the coating. Also, a tentative identification of Nb_2O_5 in the oxides formed on all four coatings was made based on the presence of an oxide phase which was yellow under sensitive tint and optically active under polarized light.

Slurry Modifiers

The baseline systems for slurry modified coatings were R512E and in-house Si-20Cr-20Fe on FS-85. The coating deposition and evaluation data are summarized in Table II and III. Most of the compositions examined behaved rather poorly. A large number of coatings had weight parity lives below 1.0 as listed in Table III. The poor performance, in many cases, could be attributed to the poor wetting and flow characteristics of the slurries during fusion. This was particularly true of coatings containing reactive metals such as W, Mo, Ti, Hf, and Zr. Many of these coatings had regions where the coating thickness was only in the range from 1 to 2 mm.

The better coatings are listed in Table II. The four best coatings were Si-20Cr-20Mn, Si-20Cr-20Fe-10HfO_2, Si-20Cr-20Fe-10B_4Si, and Si-20Cr-20Fe-5Mn. Photomicrographs of these coatings at 100X and 500X in the as-fused condition are presented in figure 11. The Si-20Cr-20Mn coating has a very thin columnar region compared to the Si-20Cr-20Fe baseline coating. Also, considerable coating buildup occurred at the edges of the Si-20Cr-20Mn coated specimen. The major differences in microstructure found in the

other coatings shown in figure 11 are coarsening of the outer zone structure in the HfO_2 modification, fine precipitates in the columnar region of the B_4Si modification and coarse rectangular grains in the outer zone of the Si-20Cr-20Fe-5Mn modification.

The performance of the four best slurry modification coatings on an absolute and weight parity basis is summarized in figure 5(c). They performed as well as or better than any of the alloy surface modifier coatings on a weight parity basis. The Si-20Cr-20Mn coating is the best coating examined to date with an average absolute life of 63 slow cycles and an average weight parity life of 3.2 cycles/mg/cm^2. These averages were reduced considerably by the premature edge failure of one specimen at 12 cycles. The other two coupons from this group survived 87 and 90 slow cycles and had weight parity lives of 4.6 cycles/mg/cm^2. With the exception of the premature failure, the observed weight parity lives for the four coatings fall well to the right of the 5 percent line for Si-20Cr-20Fe on FS-85 shown in the Weibull plot (fig. 5(b)). For the Si-20Cr-20Mn coating the observed improvement is statistically significant at the 97 percent level. All of the specimens of the four best slurry modifications failed on edges with the exception of one of the B_4Si modified coupons where an edge and surface failure were developed in the 38th cycle.

The weight change behavior of the four best slurry modified coatings explains their superiority to a certain extent. These

data are presented in figure 12 along with data for the baseline coatings. The baseline coatings show relatively large weight gains and underwent moderate to heavy spalling. The B_4Si modification had the highest weight gain of the four slurry modification coatings and spalled lightly. The other three coatings gained weight slowly and spalled only slightly. Therefore the oxidation rates of these coatings are considerably lower than the baseline coatings and they are therefore able to afford greater protection for a given coating weight.

Photomicrographs of the four best slurry modified coatings after slow cycle exposure are presented in figure 13. The Si-20Cr-20Mn coating developed a thick essentially single phase oxide with some lighter oxide particles found as inclusions as well as on the surface. The oxide formed on the edges is much thicker than on the surfaces. Also, very few diffusion zone cracks running parallel to the substrate are present. The appearance of the HfO_2 modified coating is similar to that of unmodified Si-20Cr-20Fe. The B_4Si and Mn modified Si-20Cr-20Fe coatings developed stratified oxides. The Mn modification had an optically active outer layer, a black layer, a rust colored layer, and a green inner layer when examined in cross section under polarized light. The B_4Si modification had all but the outer optically active layer. The B_4Si modification developed very few diffusion zone cracks parallel to the substrate. Also, the coating is near complete consumption which accounts for the observed surface failure.

Based on the results of polarized light metallography and XRD the principal oxides on Si-20Cr-20Mn were SiO_2 and $MnNb_2O_6$. Some Cr_2O_3 and $CrNbO_4$ was present at the coating-oxide interface and in the coating cracks. The principal oxides on Si-20Cr-20Fe-10B_4Si, Si-20Cr-20Fe-10HfO_2, and Si-20Cr-20Fe-5Mn were SiO_2, (Fe, Cr) NbO_4 and Cr_2O_3.

CONCLUSIONS

The surfaces of niobium alloys were modified prior to fused slurry silicide coating with Si-20Cr-20Fe. Edge beads were electron-beam melted on thin sheet Cb-752 and FS-85 specimens. FS-85 was surface modified with either W, $ZrO_2 \cdot CaO$ or Al_2O_3. Each of these modifiers was applied by four methods: flame spraying, roll bonding, isostatic pressing, or slurry spraying. The object of these modifications was to alter the microstructure, crack frequency, and thus the performance of the coated system. Finally, a number of slurry chemistry modifications were also examined. The applied coatings were screened by a 1370°C one-hour slow-cycle test at ambient pressure. This is a severe test since normal maximum use temperatures for this system are about 1320°C in partial vacuum and 1250°C in air. Appearance of the first Nb_2O_5 pimple was used as the coating failure criterion. This provided a conservative determination of coating life. Vendor coatings and in-house Si-20Cr-20Fe coatings were used as a baseline for comparison. Coating lives were compared on a weight parity basis,

that is, the coating life in cycles divided by the coating weight in mg/cm^2.

The following conclusions are drawn from the results of this exploratory study:

1. Slurry modification gave the greatest improvement in coating life. The Si-20Cr-20Mn coating had an average life of 63 slow-cycles to 1370°C. The weight parity life of 3.2 represents a 100 percent improvement over the baseline Si-20Cr-20Fe coating. Other coatings which showed smaller improvements were Si-20Cr-20Fe-10HfO_2, Si-20Cr-20Fe-10B_4Si, and Si-20Cr-20Fe-5Mn.

2. Edge beading by electron-beam melting was an effective method for reducing susceptibility to local coating breakdown at the edges of thin sheet material. On a weight parity basis, edge beaded Cb-752 and FS-85 specimens coated with Si-20Cr-20Fe gave lives 50 and 20 percent greater respectively than the average life obtained with R512E on these alloys.

3. The W, Al_2O_3, and $ZrO_2 \cdot CaO$ modifiers to the Si-20Cr-20Fe coating altered the crack frequency and, to some extent, the microstructure of the coating. However, the columnar structure and crack depth were not changed markedly and no universal relationship between crack frequency and life was noted. On a weight parity basis, the flame sprayed Al_2O_3 and $ZrO_2 \cdot CaO$ modifications increased life by 25 and 20 percent respectively whereas the isostatically pressed W modification gave no improvement in weight parity life.

REFERENCES

1. S. Priceman and L. Sama: Development of Fused Slurry Silicide Coatings for the Elevated-Temperature Oxidation Protection of Columbium and Tantalum Alloys. AFML-TR-68-210, December 1968.

2. H. A. Hauser and J. F. Holloway, Jr.: Evaluation and Improvement of Coatings for Columbium Alloy Gas Turbine Engine Components. AFML-TR-66-186, Part II, May 1968.

3. B. G. Fitzgerald and E. L. Rusert: Evaluation of the Fused Slurry Silicide Coating Considering Component Design and Reuse. AFML-TR-70-154, December 1970.

4. B. G. Fitzgerald: Fused Slurry Silicide Coatings for Columbium Alloy Reentry Heat Shields. Fourth Quarterly Technical Progress Narrative, NAS3-14307, July 1971.

5. R. J. Kotfila: Outer Skin Protection of Columbium Thermal Protection System (TPS) Panels. First Quarterly Technical Progress Narrative, NAS3-15546, October 1971.

6. J. F. Nejedlik and J. D. Gadd: Coatings for Long Term-Intermediate Temperature Protection of Columbium Alloys. AFML-TR-68-170, October 1968.

7. F. F. Schmidt and H. R. Ogden: The Engineering Properties of Columbium and Columbium Alloys. DMIC Report 188, September 1963.

8. L. F. Verkhorokin and N. N. Matyushenko: Poroshkovya Metallurgirja, No. 6(18), 1963.

9. V. S. Neshpor and M. I. Reznichenko: Ogneupory, No. 3, Vol. 28, p. 134 (1963).

10. R. T. Wimber and A. R. Stetson: Development of Coatings for Tantalum Alloy Nozzle Vanes. NASA CR-54529, July 1967.

11. W. B. Pearson: Handbook of Lattice Spacings and Structures of Metals, Vol. 2, Pergamon Press, London 1967.

12. I. E. Campbell and E. M. Sherwood: High-Temperature Materials and Technology. John Wiley & Sons, Inc., New York, 1967.

13. E. M. Levin; C. R. Robbins; and H. F. McMurdie: Phase Diagrams for Ceramists. The American Ceramic Society, Columbus, Ohio, 1964.

14. J. L Smialek: Exploratory Study of Oxidation-Resistant Aluminized Slurry Coatings for IN-100 and WI-52 Superalloys. NASA TN D-6329, May 1971.

15. J. C. Wurst and J. A. Cherry: The Evaluation of High-Temperature Materials. ML-TDR-64-62, Vol. II, September 1964.

16. C. E. Wicks and F. E. Block: Thermodynamic Properties of 65 Elements - Their Oxides, Halides, Carbides, and Nitrides. Bureau of Mines Bulletin 605, 1963.

17. H. E. Shoemaker and A. R. Stetson: Silicide Coatings for Tantalum and Columbium Alloys. NASA CR-72519, August 1969.

18. R. A. Perkins; C. M. Packer; and H. W. Lavendel: Fused Slurry Silicide Coatings for Tantalum Reentry Heat Shields. Third Quarterly Technical Progress Narrative, NAS3-14316, April 1971.

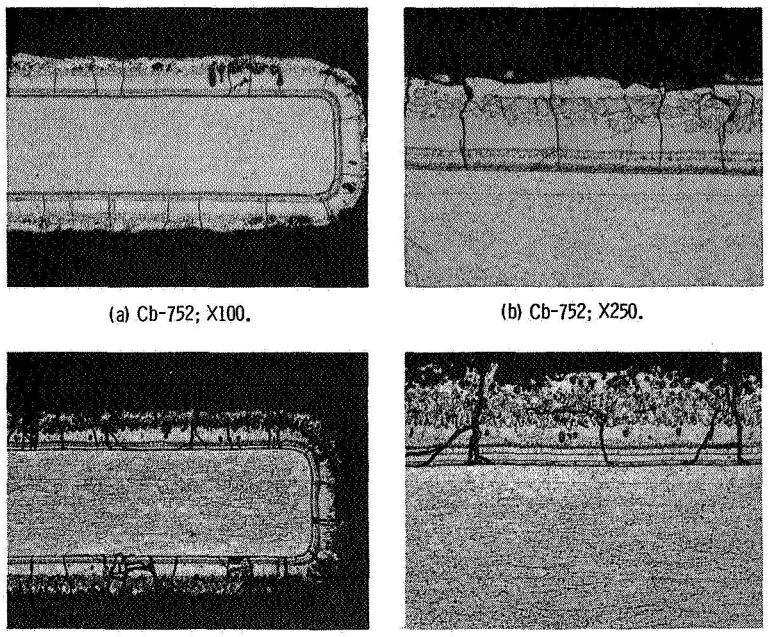

(a) Cb-752; X100.

(b) Cb-752; X250.

(c) FS-85; X100.

(d) FS-85; X250.

Figure 1. - Microstructures of R512E (Si-20Cr-20Fe) coating on niobium alloys Cb-752 and FS-85. As-coated.

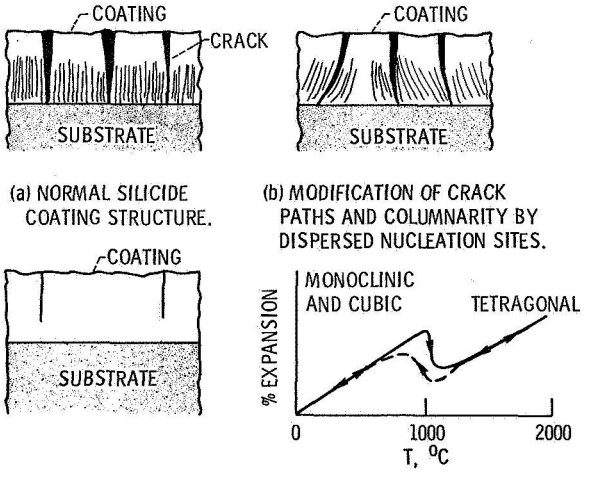

(a) NORMAL SILICIDE COATING STRUCTURE.

(b) MODIFICATION OF CRACK PATHS AND COLUMNARITY BY DISPERSED NUCLEATION SITES.

(c) MODIFICATION OF CRACK SPACING AND PENETRATION BY EXPANSION MATCHING.

(d) THERMAL EXPANSION BEHAVIOR OF $ZrO_2 \cdot CaO$.

Figure 2. - Schematics of normal coating microstructure, microstructural effects of coating modifications, and thermal expansion of zirconia.

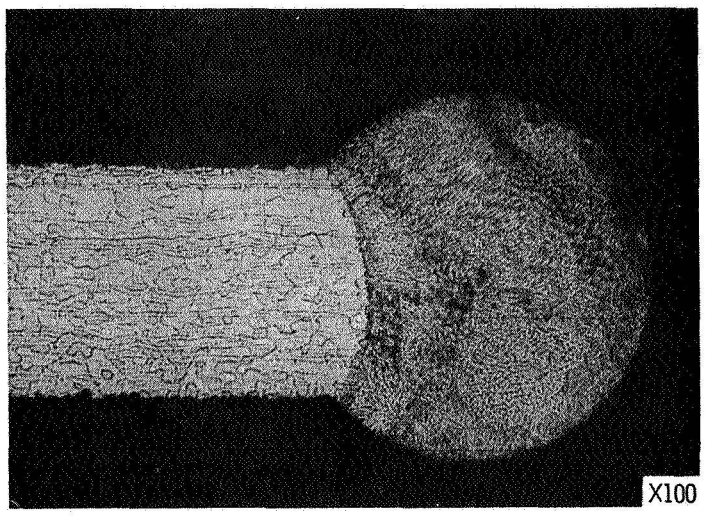

Figure 3. - Photomicrograph of cross-section E. B. melted edge bead on Cb-752.

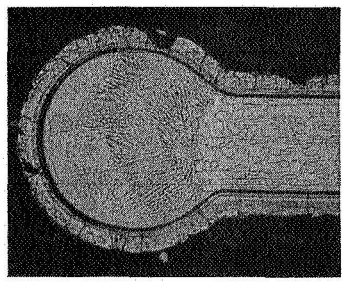

(a) Cb-752; X100.

(b) BEADED Cb-752; X250.

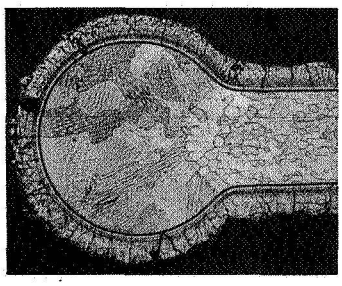

(c) BEADED FS-85; X100.

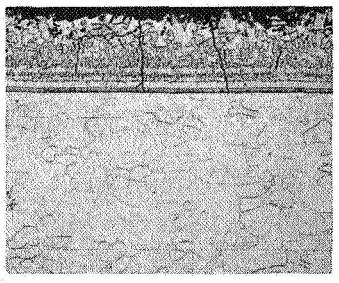

(d) FS-85; X250.

Figure 4. - Cross-sectional microstructures of unmodified Si-20Cr-20Fe on edge beaded Cb-752 and on FS-85. As-coated.

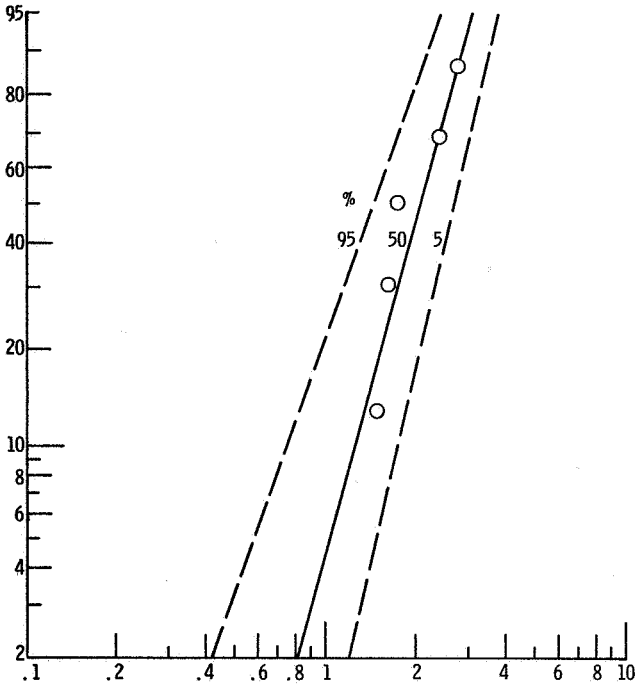

(a) R512E ON Cb-752. POINTS ARE FOR 50% LINE.

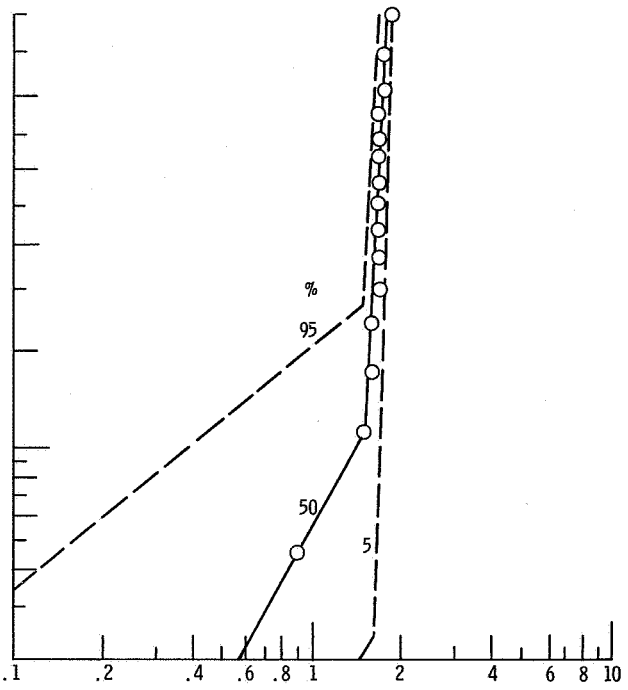

(b) WEIBULL PLOT FOR R512E AND Si-20Cr-20Fe ON FS-85.

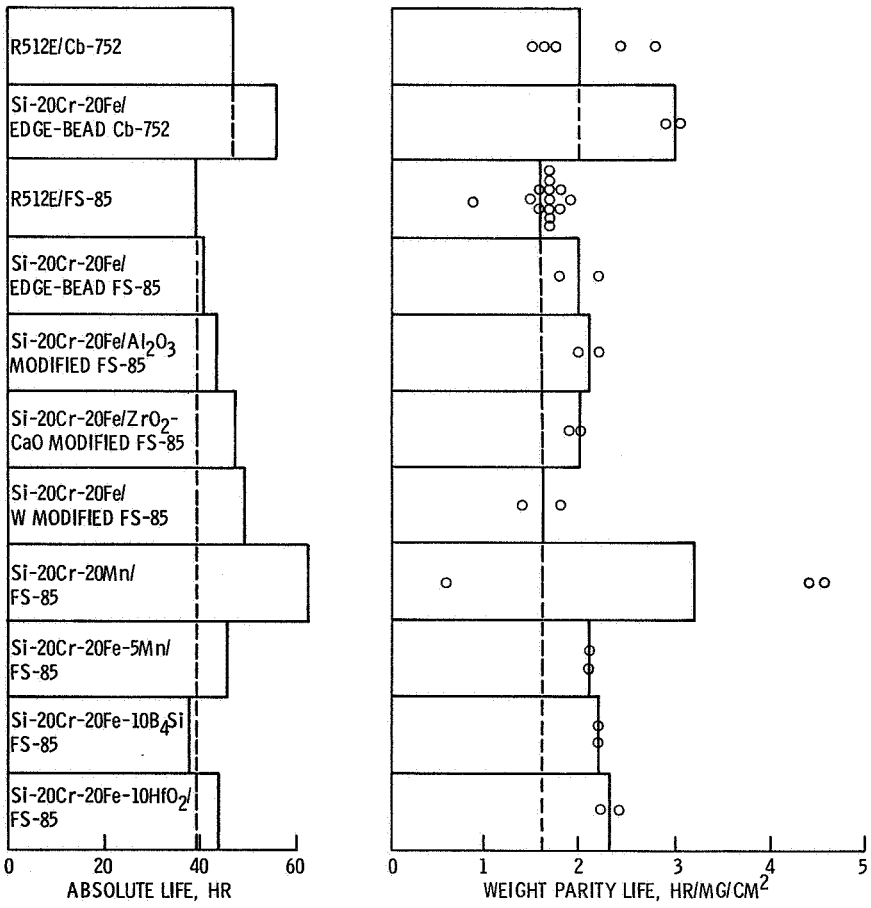

(c) COMPARISON OF 1370° C AMBIENT PRESSURE SLOW-CYCLE PERFORMANCE OF FUSED SLURRY SILICIDE COATINGS.

Figure 5. - Weibull plots for baseline coatings and coating life comparisons.

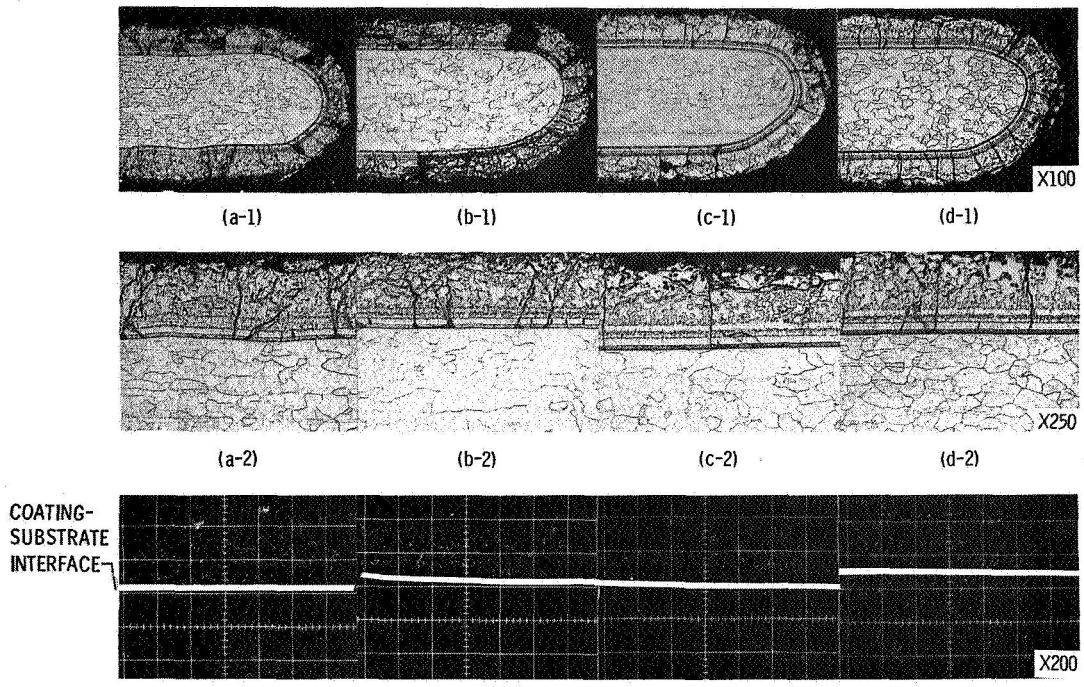

Figure 6. - Cross-sectional microstructures and aluminum raster photographs for Al_2O_3 surface modified FS-85 coated with Si-20Cr-20Fe. As-coated.

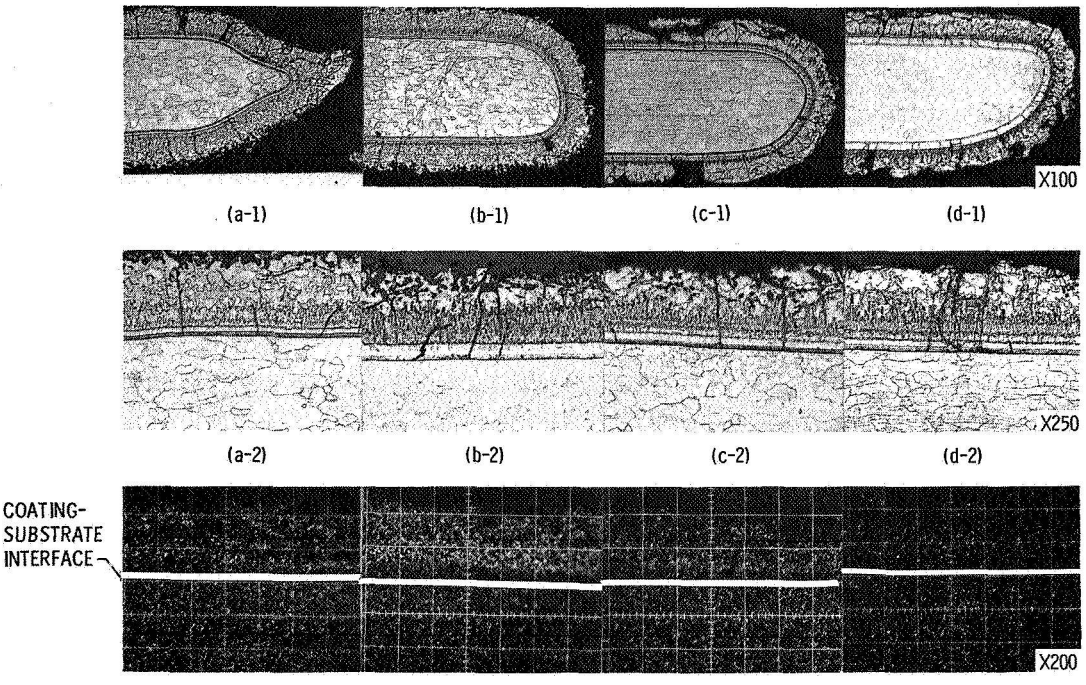

Figure 7. - Cross-sectional microstructures and zirconium raster photographs for ZrO_2-CaO surface modified FS-85 coated with Si-20Cr-20Fe. As-coated.

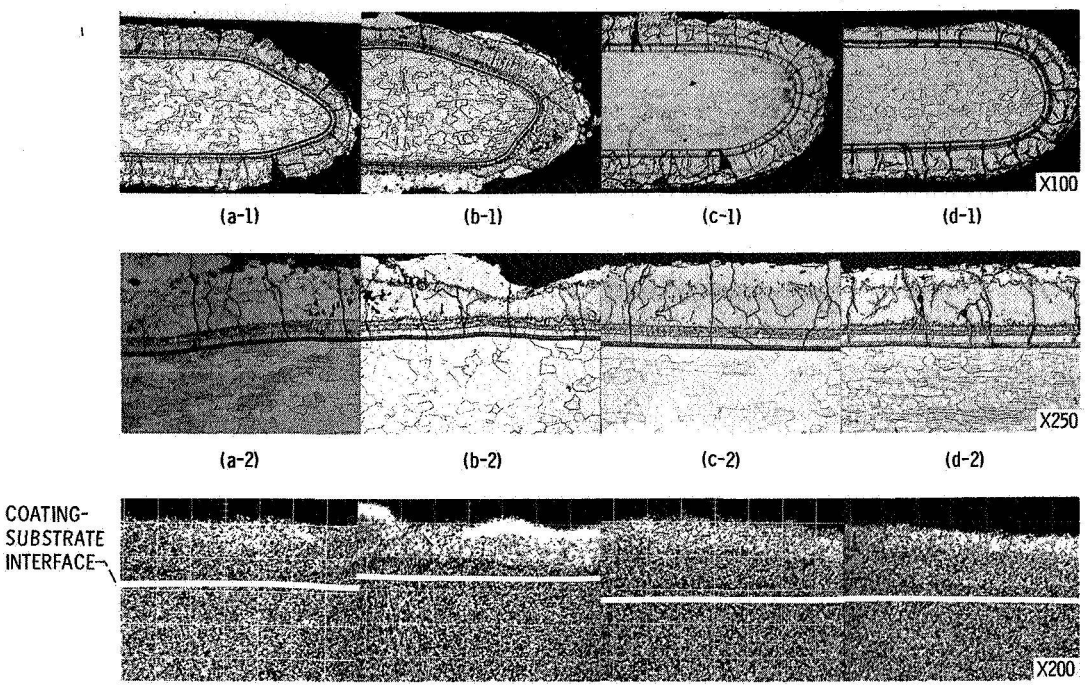

Figure 8. - Cross-sectional microstructures and tungsten raster photographs for W surface modified FS-85 coated with Si-20Cr-20Fe. As-coated.

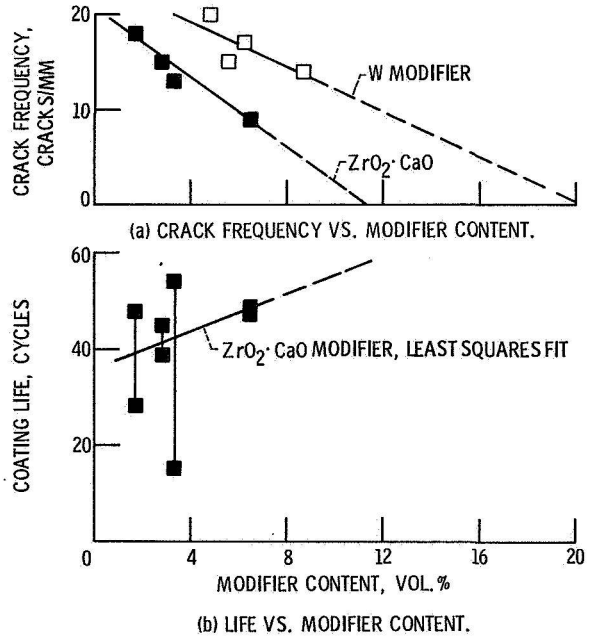

Figure 9. - The effect of modifier content on coating crack frequency and life.

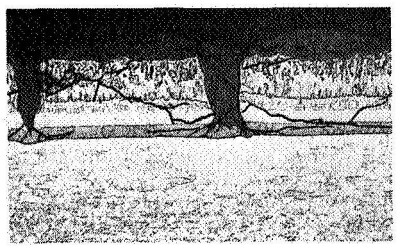

(a) R512E AFTER 46 CYCLES.

(b) FLAME SPRAY Al_2O_3 MODIFICATION AFTER 46 CYCLES.

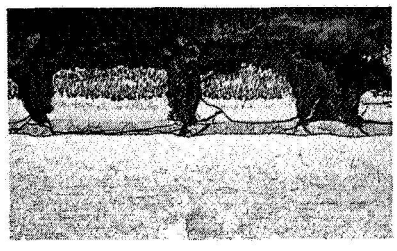

(c) FLAME SPRAY ZrO_2-CaO MODIFICATION AFTER 49 CYCLES.

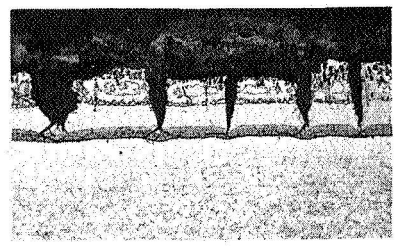

(d) ISOSTATICALLY PRESSED W MODIFICATION AFTER 57 CYCLES.

Figure 10. - Cross-sectional photomicrographs of R512E and surface modified Si-20Cr-20Fe, after 1370° C slow-cycle ambient pressure exposure to the first coating failure.

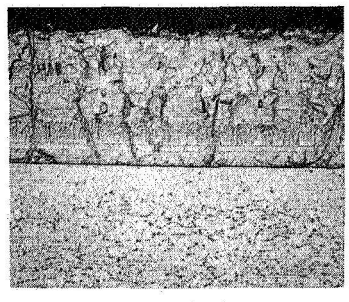

(a) Si-20Cr-20Mn, AS-COATED; X500.

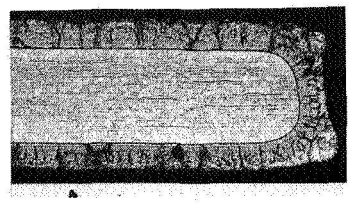

(b) Si-20Cr-20Mn, AS-COATED; X100.

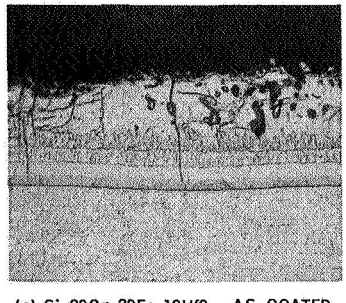

(c) Si-20Cr-20Fe-10HfO_2, AS-COATED; X500.

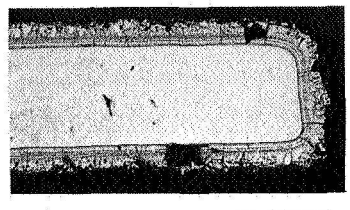

(d) Si-20Cr-20Fe-10HfO_2, AS-COATED; X100.

Figure 11. - Cross-sectional microstructures of one-step, chemically modified fused slurry silicide coatings on FS-85. As-coated.

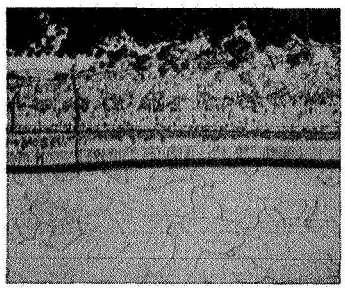

(e) Si-20Cr-20Fe-10B_4Si, AS-COATED; X500.

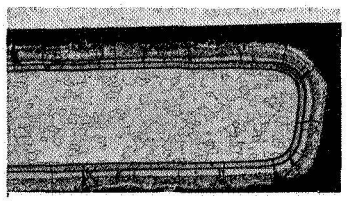

(f) Si-20Cr-20Fe-10B_4Si, AS-COATED; X100.

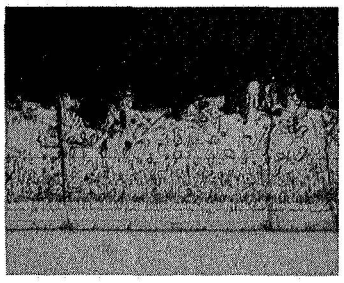

(g) Si-20Cr-20Fe-5Mn, AS-COATED; X500.

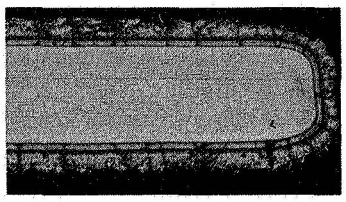

(h) Si-20Cr-20Fe-5Mn, AS-COATED, X100.

Figure 11. - Concluded.

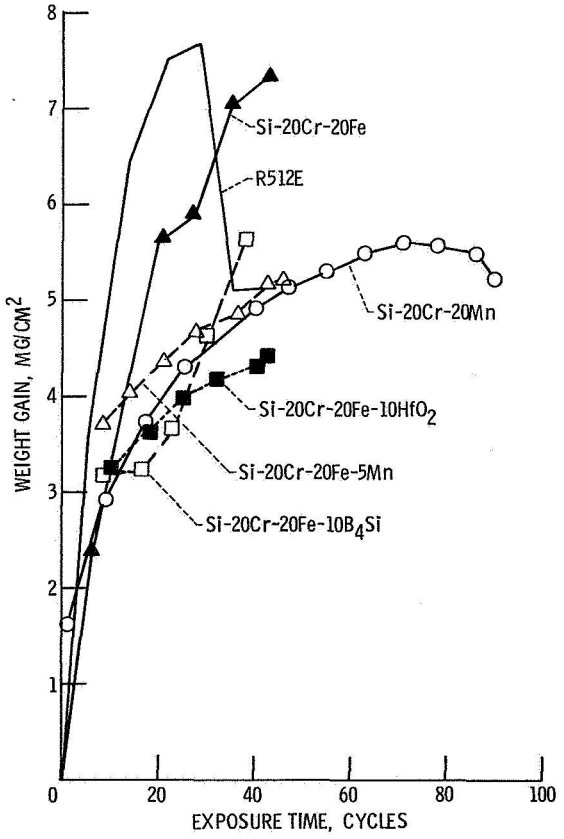

Figure 12. - Weight gain behavior of fused slurry silicides on FS-85 in the 1370^0 C slow-cycle ambient pressure test.

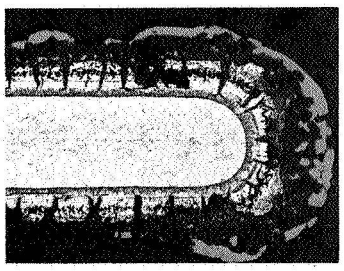

(a) Si-20Cr-20Mn AFTER 90 CYCLES; X100.

(b) Si-20Cr-20Mn AFTER 90 CYCLES; X250.

(c) Si-20Cr-20Fe-10HfO_2 after 46 cycles; X250.

(d) Si-20Cr-20Fe-10B_4Si AFTER 38 CYCLES; X250.

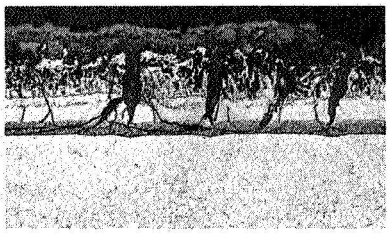

(e) Si-20Cr-20Fe-5Mn AFTER 46 CYCLES; X250.

Figure 13. - Cross-sectional microstructures of slurry chemistry modified coatings after 1370° C slow-cycle ambient pressure exposure to first coating failure.

TABLE I. - COATING DEPOSITION AND EVALUATION DATA

Coating	Substrate	Average modifier weight, mg/cm^2	Average modifier thickness, mm/side	Average green Si-20Cr·20Fe weight, mg/cm^2	Average total green coating weight, mg/cm^2	Average total fired coating weight, mg/cm^2	Average fired coating thickness, mm/side[f]	As-coated crack Frequency,[g] cracks/mm	Modifier content as-volume percent of coating	Slow cycle test life cycles	Average weight parity life, cycles/mg/cm^2	Estimated DBTT as-coated ^oC (bend angle^o)	Estimated DBTT after test ^oC (bend angle^o) (cycles tested)
Si-20Cr-20Fe	Edge beaded 0.030 cm Cb-752	--------	----------	20.1±1.0	---------	19.5±1.0	0.053	12	----	56, 59	3.0	---------	-160 (45) ⟨56⟩
R512E	0.032 cm Cb-752	--------	----------	--------	---------	24±2	0.076±0.01	13	----	$\overline{48}$(34 to 67)	2.0	---------	-195 ⟨34⟩
R512E	0.035 cm FS-85	--------	----------	--------	---------	25±2	0.082±0.01	15	----	$\overline{39}$(33 to 46)	1.6	-160	-195 ⟨46⟩
R512E	0.030 cm FS-85	--------	----------	--------	---------	25±1	0.082±0.01	13	----	$\overline{41}$(38 to 42)	1.6	-160	-195 ⟨42⟩
Si-20Cr-20Fe	0.033 cm FS-85	--------	----------	25.5±2.6	---------	22.2±1.9	0.073±0.007	16	----	$\overline{34}$(20 to 43)	1.5	---------	-160 ⟨39⟩
Si-20Cr-20Fe	↓	--------	----------	24.4±1.2	---------	21.7±0.9	----------	--	----	37, 37	1.7	-170 (75)	----------
Roll bond W[a]	↓	[b]7.2±1.5	[c]0.045±0.004	[b]25.9±0.6	[b]32.8±1.0	[b]30.5±1.0	[d]0.081±0.002	20	4.8	19, 48	1.1	---------	-160 ⟨25⟩
Roll bond Al_2O_3	↓	[b]1.2±0.1	[c]0.044±0.004	[b]26.4±2.2	[b]27.7±2.4	[b]22.4±0.7	[d]0.072±0.004	26	4.4	6, 43	1.1	---------	-170 ⟨43⟩
Roll bond ZrO_2·CaO	↓	[b]1.1±0.1	[c]0.048±0.004	[b]25.5±0.5	[b]26.6±0.5	[b]23.5±0.7	[d]0.073±0.002	15	2.8	39, 45	1.8	---------	-195 ⟨45⟩
Flame spray W	↓	14.8±3.3	0.050±0.01	25.0±1.2	40.5±4.5	36.8±2.5	0.091±0.011	14	8.7	24, 34	0.8	---------	-195 ⟨24⟩
Flame spray Al_2O_3	↓	3.8±1.5	0.040±0.01	26.6±1.3	30.4±2.3	21.3±2.5	0.064±0.003	28	15.6	42, 46	2.1	---------	-170 ⟨42⟩
Flame spray ZrO_2·CaO	↓	3.2±1.3	0.045±0.01	26.5±1.6	29.4±2.2	24.2±0.7	0.091±0.008	9	6.5	47, 49	2.0	---------	-195 ⟨47⟩
Isostatic press W	↓	7.5±1.0	[e]0.029±0.005	26.0±1.7	33.8±2.2	32.0±1.3	0.073±0.006	15	5.5	44, 57	1.6	---------	-170 ⟨44⟩
Isostatic press Al_2O_3	↓	1.0±0.2	[e]0.064±0.003	27.2±1.8	28.3±2.1	23.3±0.8	0.075±0.006	22	3.6	15, 30	1.0	---------	-180 ⟨15⟩
Isostatic press ZrO_2·CaO	↓	0.7±0.3	[e]0.044±0.001	26.7±1.3	27.4±1.1	24.2±0.8	0.079±0.004	18	1.7	28, 48	1.6	---------	-170 ⟨28⟩
Slurry spray W	↓	8.3±0.4	0.047±0.003	24.6±1.4	32.3±1.6	30.2±1.7	0.072±0.004	17	6.2	12, 21	0.6	---------	-170 ⟨12⟩
Slurry spray Al_2O_3	↓	1.5±0.5	0.045±0.005	26.6±0.6	28.2±0.6	23.5±0.3	0.072±0.002	20	5.5	27, 47	1.6	---------	-180 ⟨47⟩
Slurry spray ZrO_2·CaO	↓	1.5±0.2	0.048±0.001	26.7±3.7	28.0±1.1	24.6±0.6	0.085±0.001	13	3.3	15, 54	1.4	---------	-160 ⟨54⟩
Si-20Cr-20Fe	Edge beaded 0.033 cm FS-85	--------	----------	24.2±0.4	---------	20.8±0.4	0.062±0.02	18	----	37, 45	2.0	---------	---------

[a]Modifiers were overcoated with Si-20Cr-20Fe.
[b]Weight based on area after rolling.
[c]Thickness as measured prior to rolling.
[d]Thickness based on increase after roll bonding.
[e]Thickness after Isostatic pressing.
[f]Determined by hand micrometer.
[g]From through coating cracks on X100 cross-section micrographs.

TABLE II. - COATING CHEMISTRY MODIFICATIONS ON FS-85

Coating composition	Green coating weight, mg/cm^2	Firing cycle	Fired coating weight, mg/cm^2	Coating thickness,[a] mm/side	Coating crack frequency, cracks/mm[b]	1370° C slow cycle life	Weight parity life, cycles/mg/cm^2	Comments
Si-20Cr-20Fe			25	0.10	15	40	1.6	Baseline system
Si-20Cr-20Fe-15Al_2O_3	23.1±0.9	1415° C Vac	12.5±0.4	0.04±0.02	15	10, 17	1.1	
Si-20Cr-20Fe-10HfO_2	23.2±0.4	1415° C Vac	19.3±0.3	0.07±0.01	13	46, 42	2.3	
Si-20Cr-20Co	22.6±1.1	1415° C Vac	20.1±0.2	0.06±0.01	14	34, 36	1.7	
Si-20Cr-20Co	22.6±1.1	1400° C Ar	20.9±0.7	0.07±0.01	17	28, 28	1.3	
Si-10Cr-10Fe-20CoAl	22.1±2.3	1415° C Vac	18.8±0.8	0.06±0.01	17	21, 15	1.0	
Si-20Ti-20Co	23.6±0.8	1415° C Vac	22.2±1.5	0.05±0.01	10	21, 32	1.2	
Si-20Cr-20Fe-10B_4Si	21.7±3.1	1415° C Vac	17.2±0.5	0.065±0.005	17	38, 38	2.2	
Si-20Cr-20Fe-10B_4Si	21.7±3.1	1400° C Ar	18.2±0.7	0.075±0.01	17	12, 51	1.8	
Si-20Cr-20Fe-10VSi_2	26.2±2.8	1415° C Vac	24.8±2.1	0.09±0.01	20	45, 45	1.8	
Si-20Cr-20Fe-5VSi_2	26.4±1.6	1415° C Vac	25.5±1.6	0.09±0.01	13	28, 28	1.1	
Si-20Cr-20Fe-10VSi_2	24.0±0.6	1400° C Ar	22.7±0.3	0.080±0.005	17	2, 45	1.1	
Si-20Cr-20Fe-10W	27.0±1.4	1415° C Vac	25.0±0.6	0.08±0.01	18	43, 43	1.7	
Si-15Cr-15Fe-10W	27.7±2.4	1415° C Vac	27.2±0.9	0.09±0.01	19	38, 38	1.4	
Si-20Cr-20Mn	21.2±1.0	1415° C Vac	14.6±0.3	0.06±0.03	11	26, 28	1.9	
Si-20Cr-20Mn	21.2±1.0	1370° C Ar	19.4±0.5	0.075±0.005	15	12, 87, 90	3.2	Forms viscous glass
Si-20Ti-20Mn	22.5±1.5	1415° C Vac	16.7±1.4	0.05±0.01	7	14, 20	1.0	
Si-20Ti-20Mn	22.5±1.5	1370° C Ar	20.6±0.5	0.06±0.01	19	20, 20	1.0	Forms fluid glass
Si-20Cr-20Fe-5Mn	22.8±1.2	1370° C Ar	21.6±0.4	0.065±0.01	13	46, 46	2.1	
Si-15Cr-15Co-10Mn-10W	22.5±1.0	1415° C Vac	20.6±0.2	0.06±0.02	16	33, 33	1.6	

[a]Based on metallographic measurements.

[b]From through coating cracks on X100 cross-section micrographs.

TABLE III. - COATING CHEMISTRY MODIFICATIONS ON FS-85 WHICH GAVE WEIGHT PARITY LIVES LESS THAN 1.0

Coating Composition	Green coating weight, mg/cm^2	Firing Cycle	Firing coating weight, mg/cm^2	Coating thickness, mm/side[a]
Si-20Cr-20Fe-20ZrO_2	22.6±0.7	1415° C Vac	13.6±0.3	0.045±0.015
Si-10Cr-10Fe-20CoAl	22.1±2.3	1400° C Vac	19.9±1.6	0.07±0.01
Si-10Cr-10Fe-20NiAl	23.5±0.8	1415° C Vac	19.9±2.2	----------
Si-10Cr-10Fe-20NiAl	23.5±0.8	1400° C Ar	21.5±0.2	0.10±0.01
Si-15Cr-15Fe-10W-10VSi_2	22.2±0.4	1405° C Vac	19.5±0.3	0.07±0.01
Si-15Cr-15Fe-10W-10VSi_2	22.5±0.3	1405° C Ar	21.0±0.1	0.065±0.01
Si-15Cr-15Fe-10W-10Ti-10VSi_2	22.1±1.0	1415° C Vac	18.7±0.4	0.04±0.03
Si-15Cr-15Fe-10W-10Ti-10VSi_2	22.0±0.5	1405° C Ar	20.4±0.2	0.045±0.03
Si-15Cr-15Fe-10Mo-10Ti-10VSi_2	22.8±0.7	1415° C Vac	19.4±0.6	0.04±0.025
Si-15Cr-15Fe-10Mo-10Ti-10VSi_2	22.7±0.6	1405° C Ar	21.1±0.2	0.04±0.03
Si-15Cr-15Fe-10Ti-10VSi_2	23.8±0.4	1405° C Vac	20.9±0.7	0.07±0.01
Si-15Cr-15Fe-10Ti-10VSi_2	23.5±1.0	1405° C Ar	21.8±0.4	0.07±0.02
Si-15Cr-15Ti-10Mn-10W	22.4±1.1	1415° C Ar	20.0±0.4	----------
Si-20Fe-20Mn	24.0±0.6	1410° C Ar	22.1±0.5	0.065±0.05
Si-20Ti-20Cr-5Mn	23.3±0.3	1370° C Ar	21.3±0.3	0.05±0.035
Si-10Cr-10Fe-20Ti	23.2±1.6	1415° C Vac	20.9±0.6	----------
Si-15Cr-15Fe-20Nb	23.1±1.1	1415° C Vac	20.1±0.2	----------
Si-20Ti-20Cr	23.6±0.8	1405° C Ar	21.5±0.3	0.07±0.03
Si-20Zr-20Mn	22.8±1.0	1370° C Ar	20.9±0.6	0.06±0.01
Si-20Zr-20Mn	22.8±1.0	1415° C Vac	16.3±0.3	0.055±0.005
Si-20Hf-20Mn	24.1±3.8	1370° C Ar	21.8±0.8	0.06±0.01
Si-20Hf-20Mn	24.1±3.8	1415° C Vac	17.1±0.7	----------

[a]Based on metallographic measurements.